Star formation news letter # 273 6-10本目

大橋聡史

The effects of a magnetic field on planetary migration in laminar and turbulent discs

Megan L. Comins[1], Marina M. Romanova[1], Alexander V. Koldoba[2,3], Galina V. Ustyugova[4], Richard V.E. Lovelace[1,5]

Accepted by MNRAS
http://arxiv.org/pdf/1508.03241

円盤での惑星はmigrationでどのように軌道が変化するのか磁場を入れて調べた

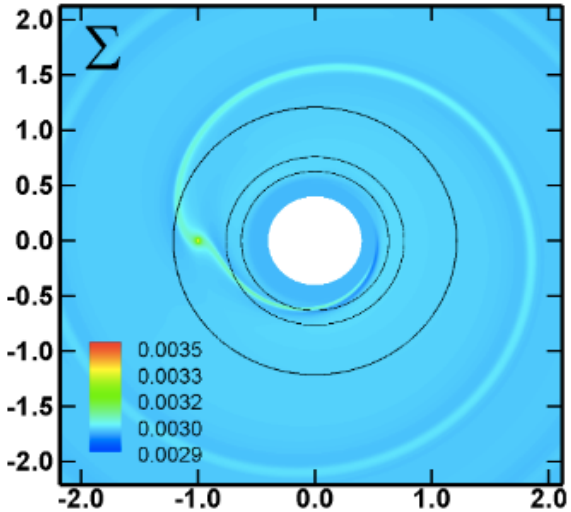

地場なし

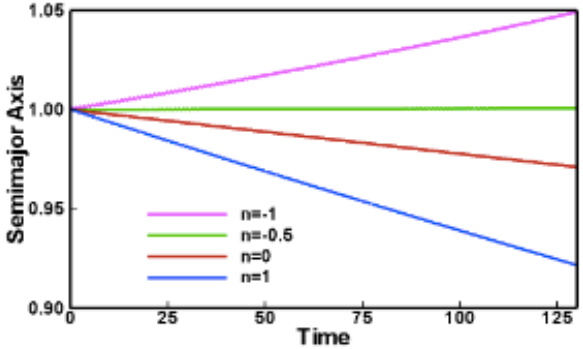

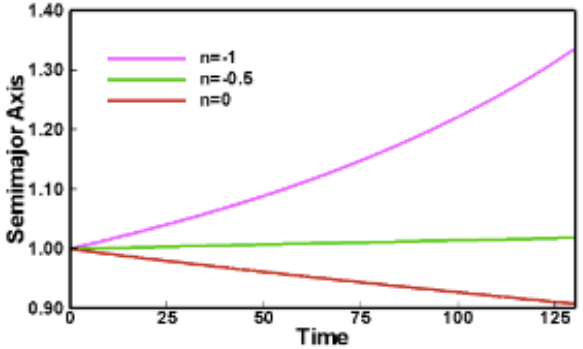

時間とともに磁場と密度はchaoticになる

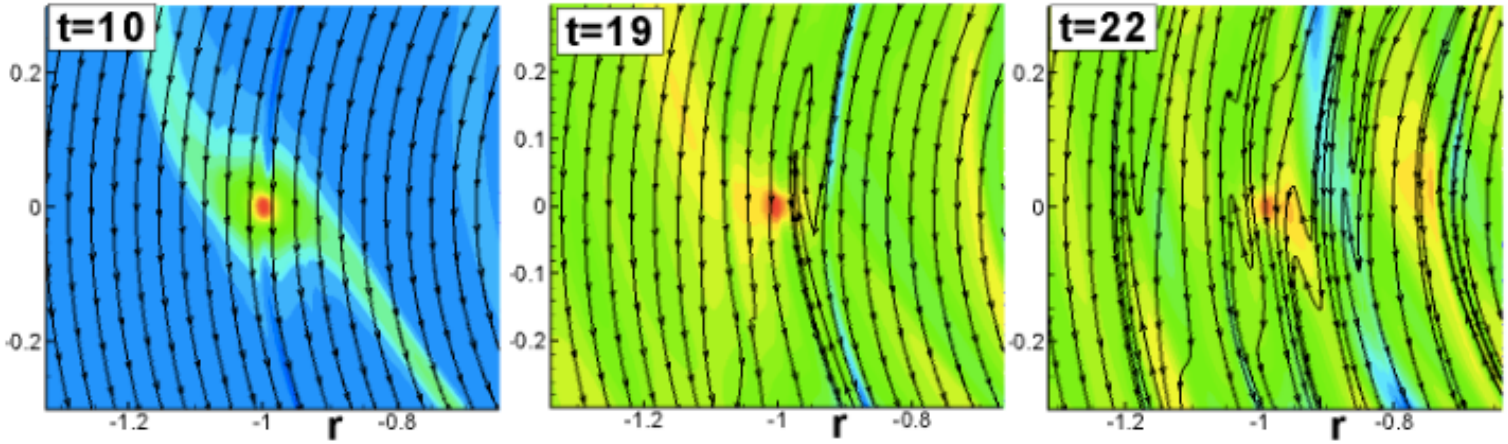

密度と磁場の分布（パワーロー）によってmigrationは変化

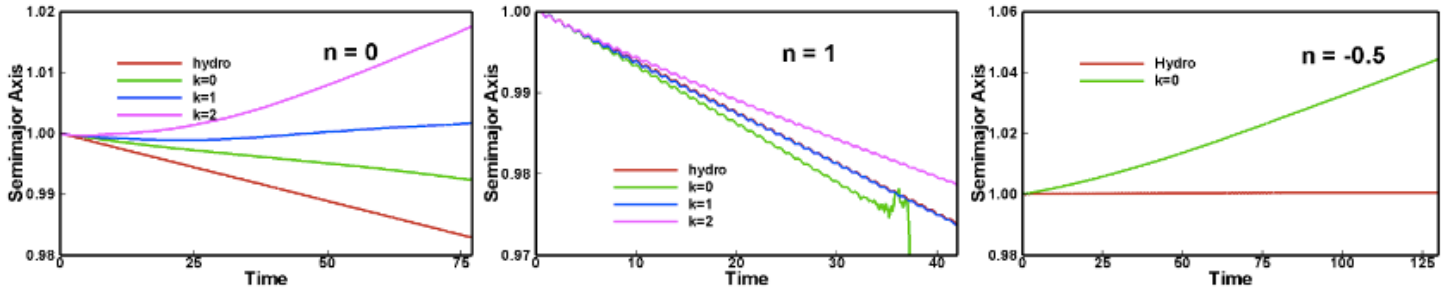

プラズマβを変えてもmigrationの様子は変化
時間が経つとturbulentに

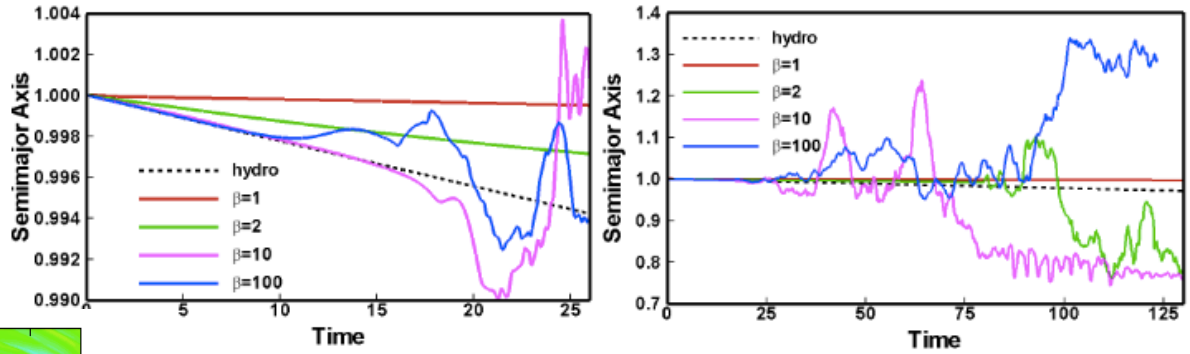

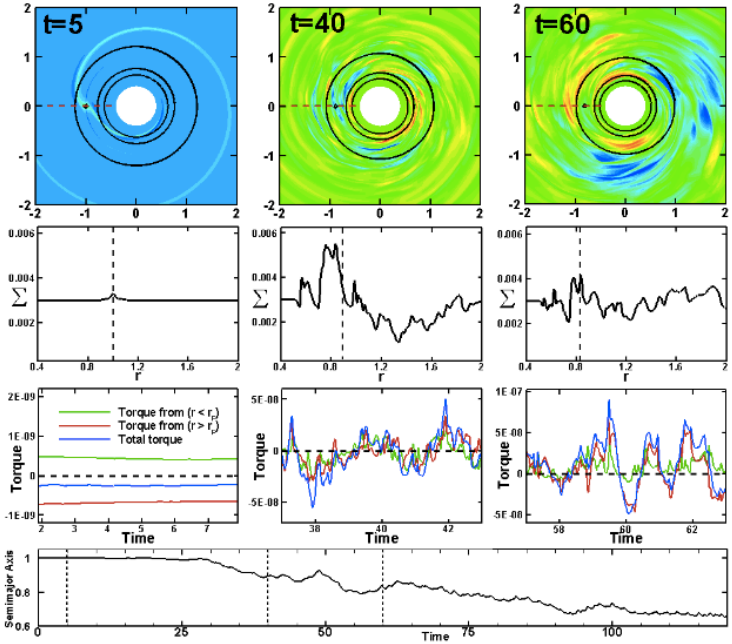

密度一様でβ=100で時間進化を見た
MRIによるturbulentがt=10くらいから始まる
MRIの初期は密度変動が小さいものが短い間隔で起こる
後期段階では大きな変動が周期的

短い密度波の振動を起こさせた場合、振動する

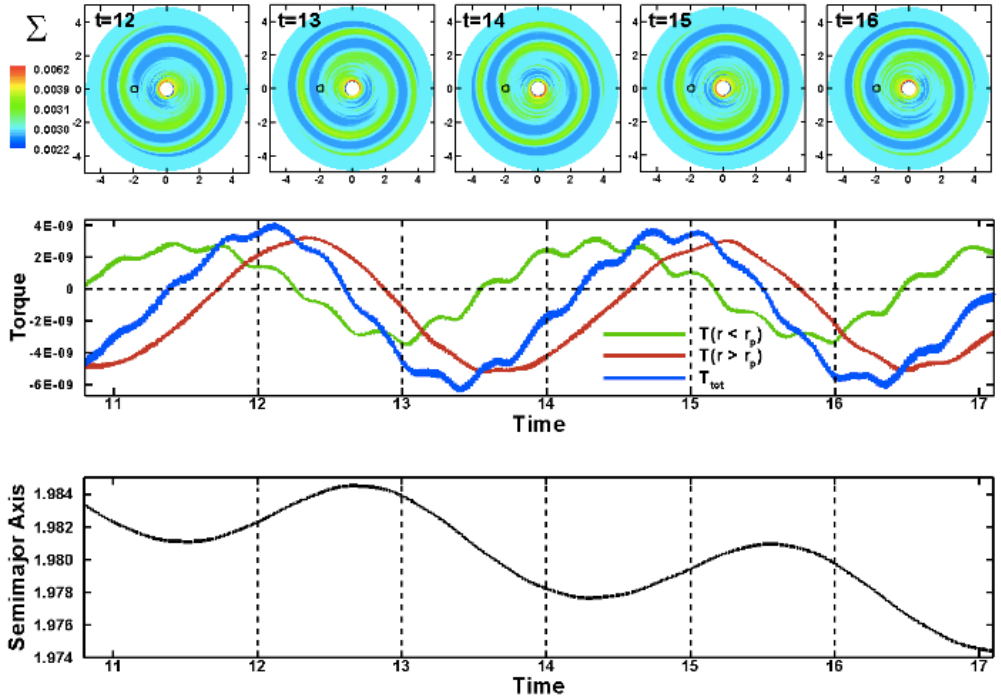

大きな密度波の振動を起こさせた場合、振動する

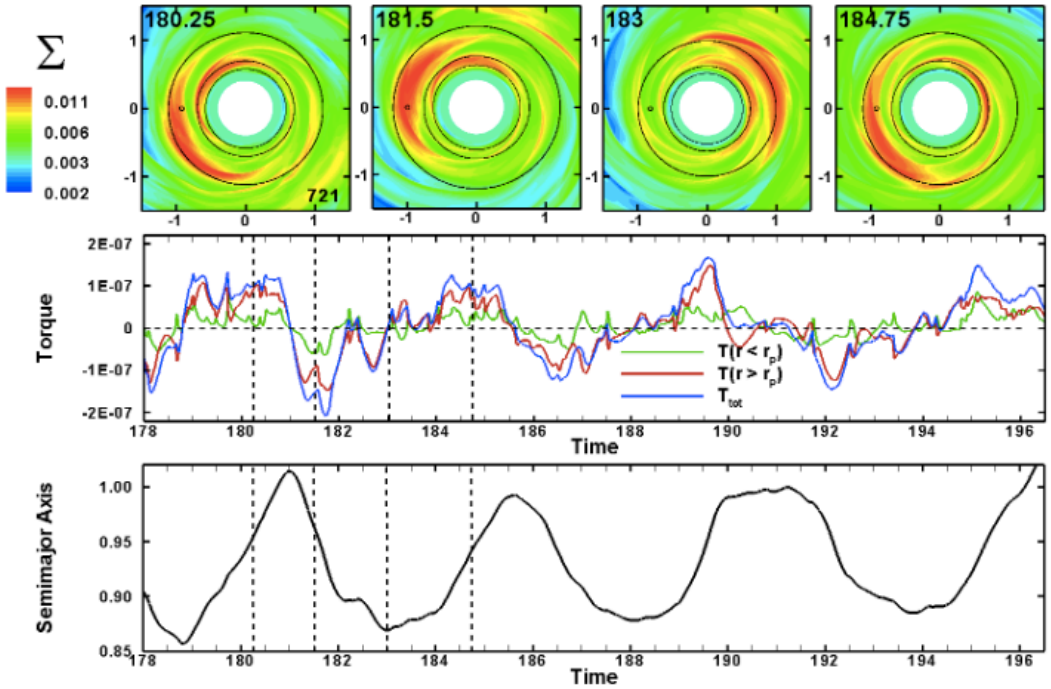

The Distribution of Main Sequence and Pre-Main Sequence Stars in the Young Anti-center Cluster NGC 2401

T.J. Davidge[1]

Accepted by PASP
http://arxiv.org/pdf/1508.07976

GenimiでNGC 2401のMSとcandidate PMSの分布を調べた
MSは中心に位置し、cPMSの分布はflatになっている
→質量損失が激しくおこり、構造が変化したりsecular dynamical evolutionではなく
もし大質量星が高密度な原始星団の中心で形成されたら自然に生じるprimordialな
Sub-clusteringを示唆している

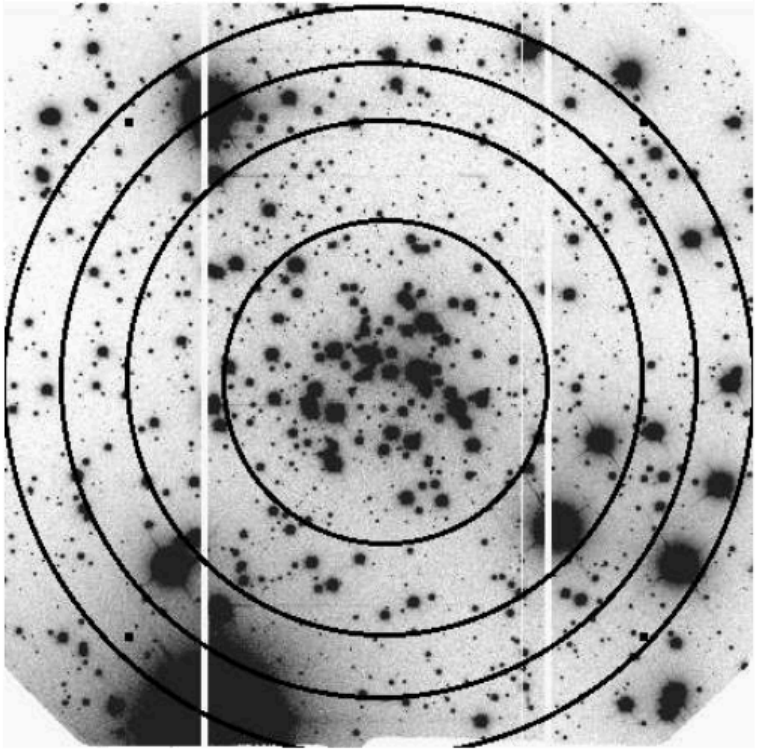

Fig. 2.— Region boundaries. Region 5 encompasses the area that is external to the largest annulus. The backdrop is the long exposure g' GMOS image, which covers 5.5×5.5 arcmin^2. North is at the top, and east is to the right. The two prominent vertical stripes are gaps between CCDs.

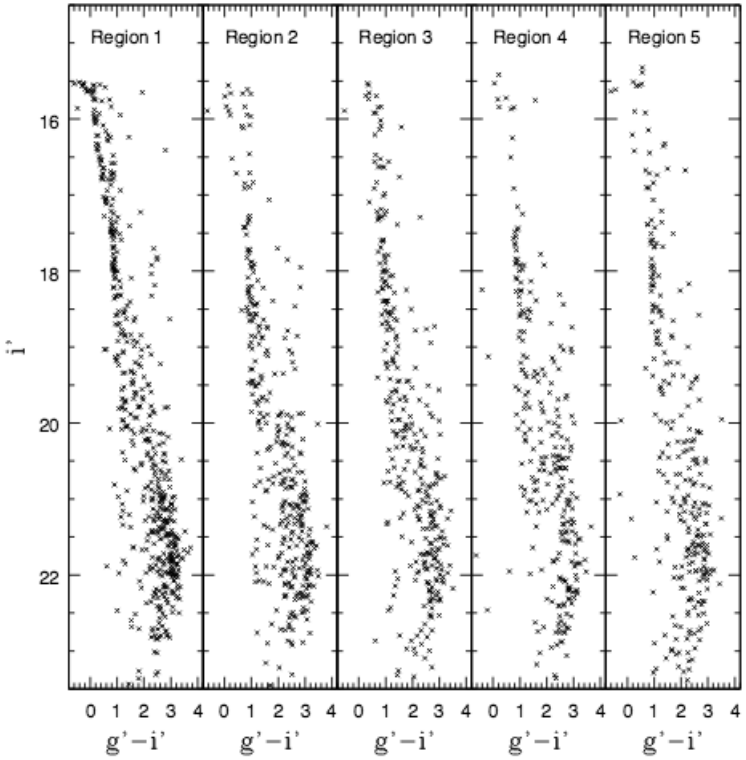

Fig. 1.— Color-magnitude diagrams. The CMDs sample equal area regions that are centered on the main concentration of bright stars in NGC 2401. The photometry of objects with $i' < 17.5$ is from the short exposure images, and the bright limit is defined by detector saturation. Number counts suggest that Regions 1 – 3 contain objects that belong to NGC 2401, whereas Regions 4 and 5 contain few cluster sources.

The Distribution of Main Sequence and Pre-Main Sequence Stars in the Young Anti-center Cluster NGC 2401

T.J. Davidge[1]

外側ではMSとPMSの分布はほぼ一致しているので、mass segregationやmass lossの影響は考えにくい,
もともと中心ほど高密度でmassive starが素早くできると考えればよい

NGC2401 ~ a few tens Myr
Region 4+5はほぼPMS

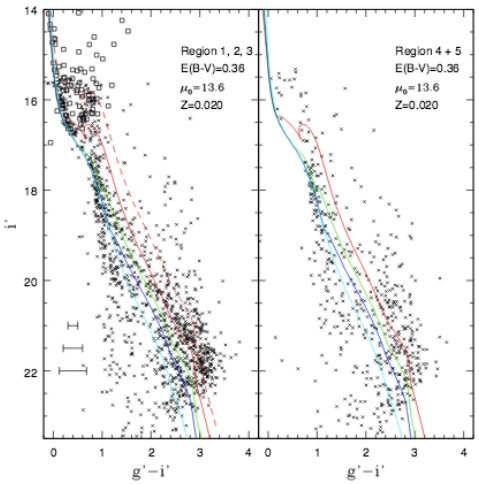

Fig. 4.— Comparisons with isochrones. The $(i', g'-i')$ CMDs of Regions 1, 2, and 3 (left hand panel) and Regions 4 and 5 (right hand panel) are shown. Regions 1, 2, and 3 together sample an area that is 50% larger than that covered by Regions 4 and 5. The error bars in the left hand panel show the $\pm 2\sigma$ dispersion in $g'-i'$ of sources with $g'-i' \sim 3$ obtained from artificial star experiments. The open squares are photometric measurements from Baume et al. (2006) that have been tranformed into the SDSS system. Isochrones from Bressan et al. (2012) that have Z=0.020 and ages of 10 (red), 20 (green), 32 (blue), and 71 (cyan) Myr are shown. The adopted distance modulus is 13.6, and the color excess is that measured by Baume et al. (2006). The dashed red line is the 10 Myr sequence shifted to brighter magnitudes by 0.75 magnitudes to simulate a sequence of unresolved equal-mass binaries.

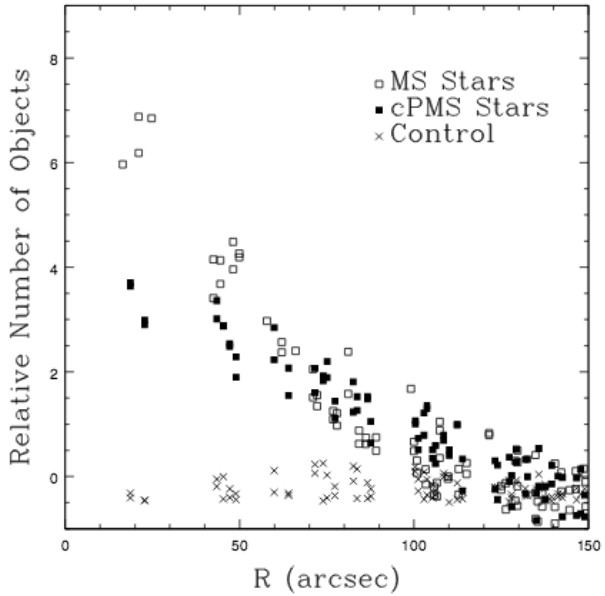

Fig. 7.— Radial profiles of the images in Figure 6. The solid squares show number counts for the cPMS sample, while the open squares show number counts for the MS stars. The profiles have been corrected for field star contamination by subtracting number counts made in Regions 4 and 5, and the results have been scaled to balance the total number of sources in each sample. The distribution of MS stars has a prominent central cusp, whereas the cPMS stars are not as centrally concentrated. The crosses show the radial distribution of objects that have the same brightness range as cPMS objects, but bluer colors. These sources have a more-or-less uniform on-sky distribution, indicating little or no contamination from cluster stars in this brightness and color range.

2点相関関数(1がuniform)
Binary (<1.5”)ではMSが3倍多い
質量の違いを見ているだけ？

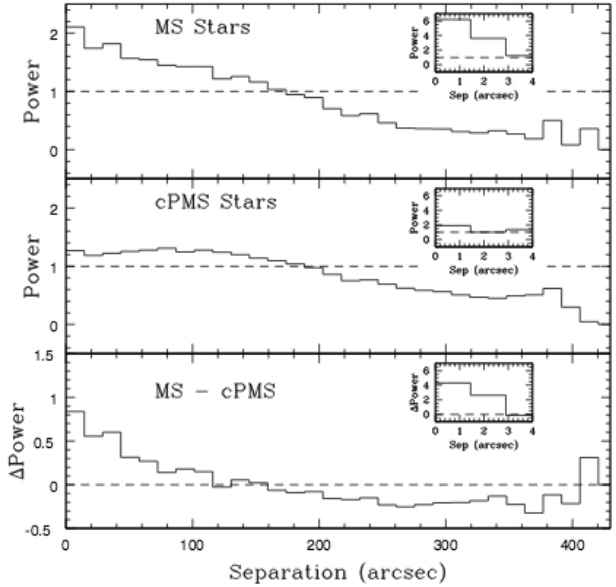

Fig. 8.— Correlation functions. The y-axis shows the number of all possible pairings of objects per 15 arcsec separation interval, divided by the separation function of a randomly distributed ensemble of stars and scaled to the total number of pairings. The TPCF of a uniformly distributed population then has a uniform power = 1. Correlation functions with finer angular binning and restricted to separations < 4 arcsec, which is the angular range where binaries and compact sub-structures will be resolved in NGC 2401, are shown in the insets. The difference between the TPCFs of the MS and cPMS samples is shown in the bottom panel.

High-Temperature Ionization in Protoplanetary Disks

Steven J. Desch[1] and Neal J. Turner[2]

Accepted by The Astrophysical Journal
http://xxx.lanl.gov/pdf/1508.07878

円盤の近傍 a few AU(>500 K)における電子とイオンのアバンダンスの計算を行った
今まではgas-phaseの計算だけ（サハの公式)だったが、dustでの表面反応を追加
イオン化ポテンシャルよりもgrains上での仕事関数（）に依存
800 Kを超えると電化のアバンダンスが急激に増える
これらを計算するとdisk dead zoneのinnder edgeは1000 Kくらい
これはambipolar diffusionで決まる

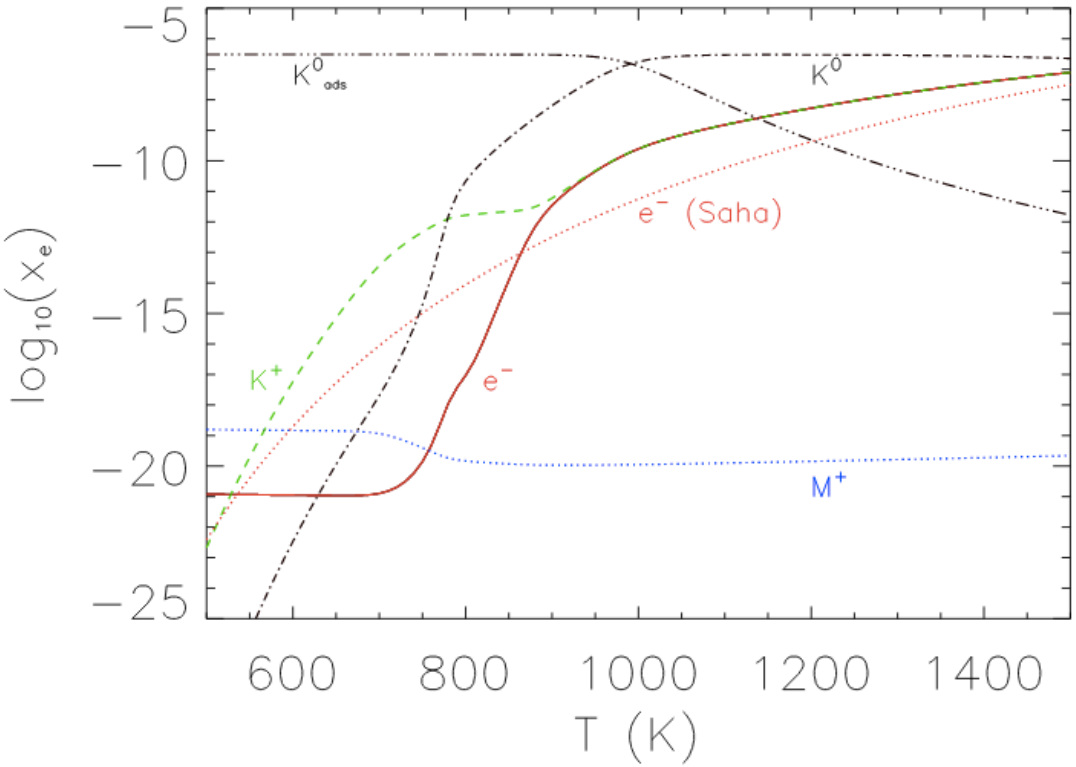

High-Temperature Ionization in Protoplanetary Disks

Steven J. Desch[1] and Neal J. Turner[2]

Dead zone 原始星近くでは高密度でオン-電子再結合で電離度が低くMRIが起こらない

エルサッサー数=0以上で不安定
Ambipolarが決めて

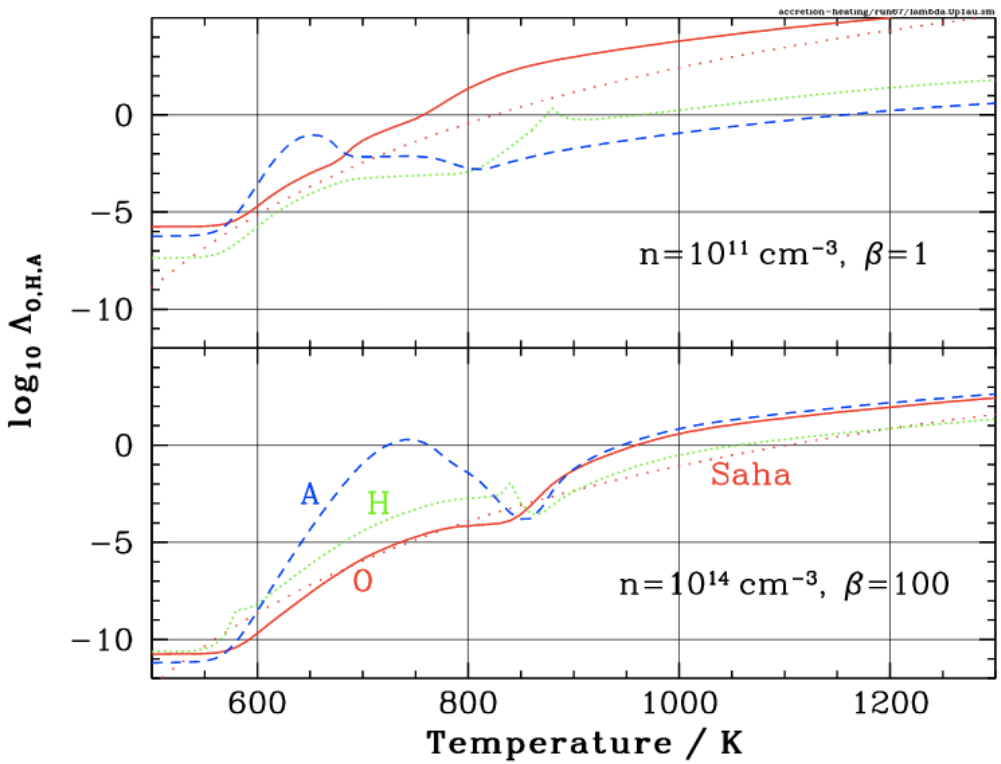

星表面へのガスのloading

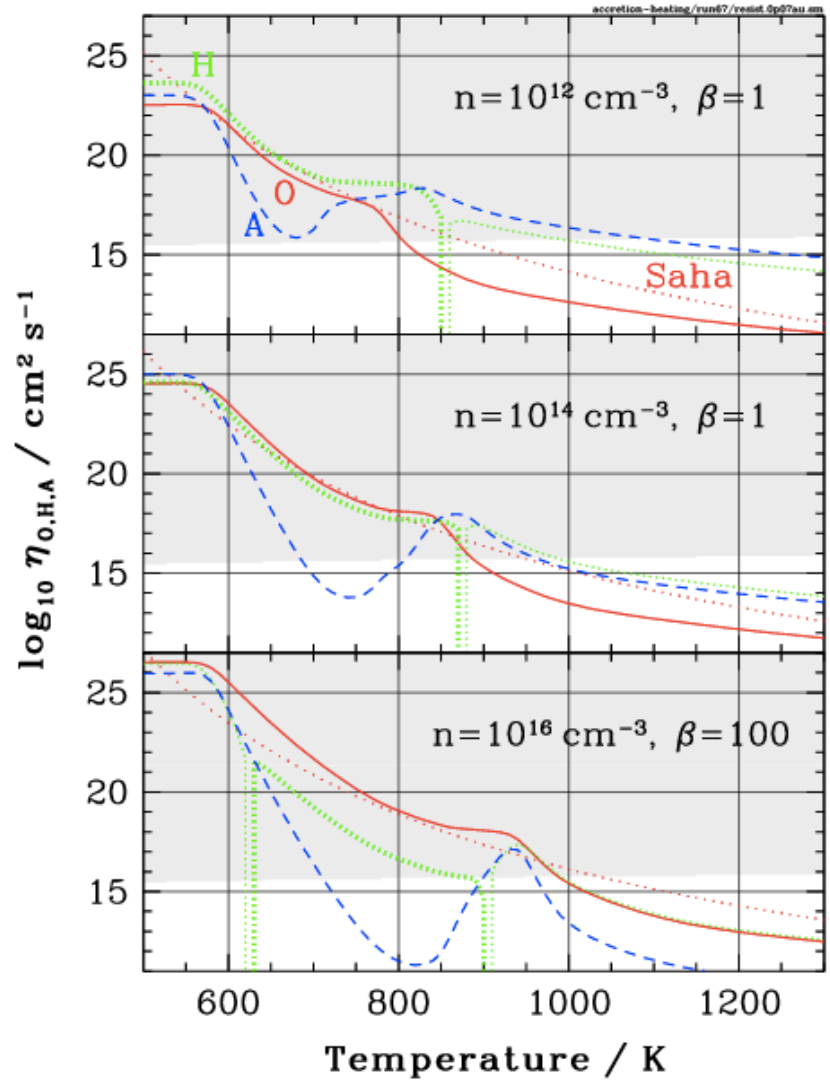

Physical environment of massive star-forming region W42

L. K. Dewangan[1], A. Luna[1], D. K. Ojha[2], B. G. Anandarao[3] and Y. D. Mayya[1]

Accepted by The Astrophysical Journal
http://arxiv.org/pdf/1508.04425v1.pdf

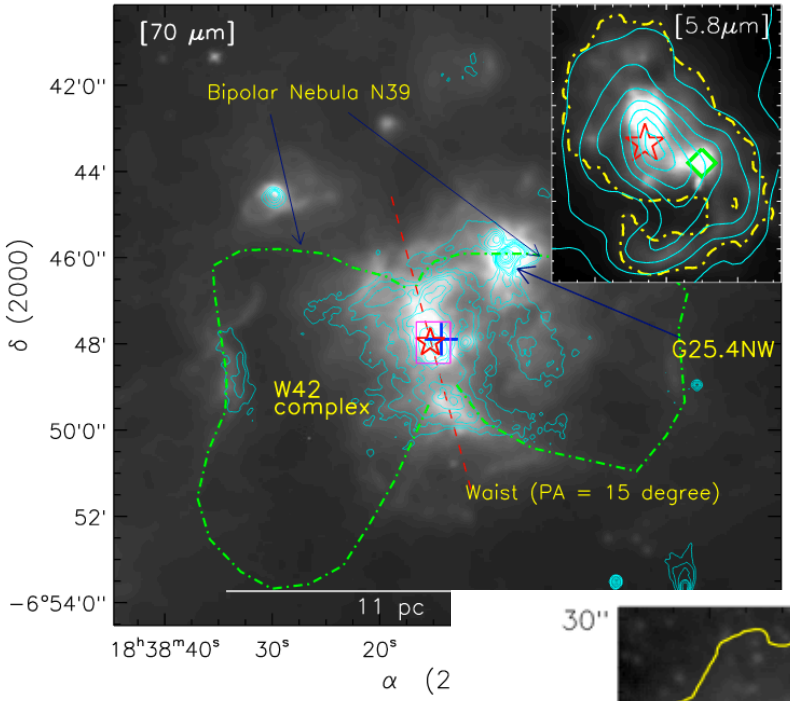

多波長(Herschel Spitzer VLT 2MASSなど)
でW42 complexを調べた

Contour 20 cm
Star O5-O6 star
+ IRAS点
メタノールメーザー

Multiple star system

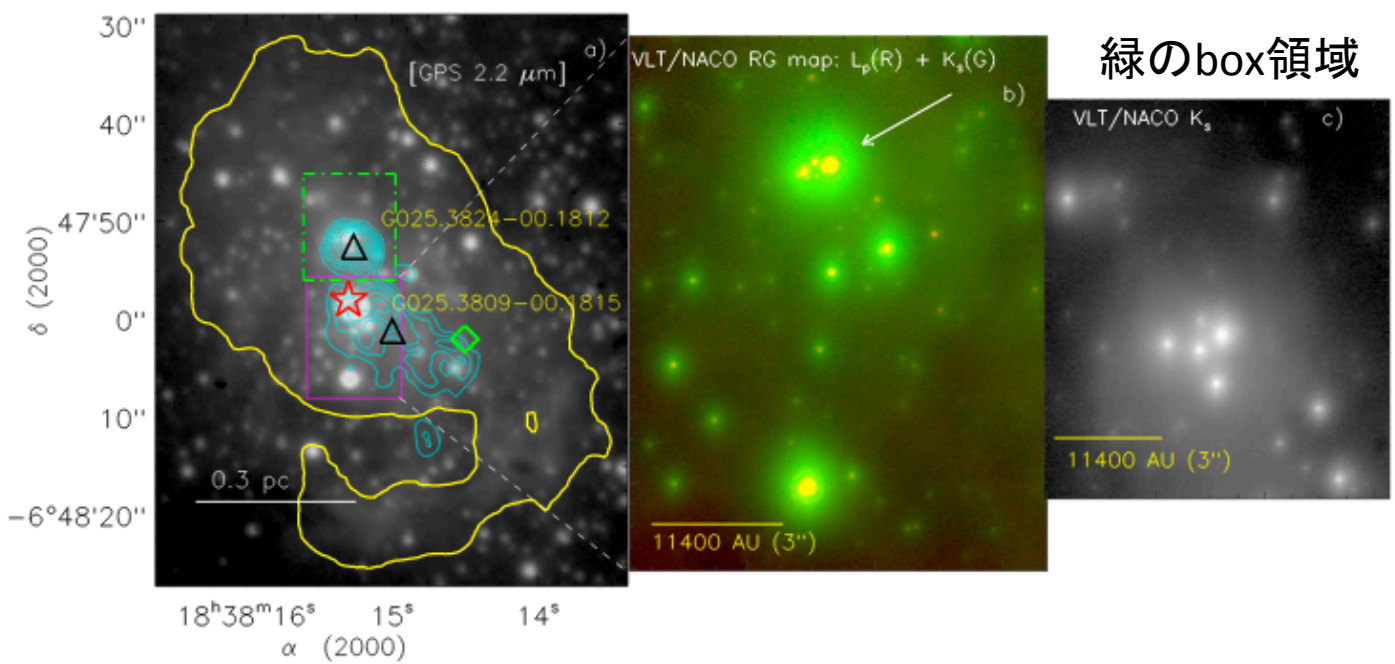

緑のbox領域

Physical environment of massive star-forming region W42

L. K. Dewangan[1], A. Luna[1], D. K. Ojha[2], B. G. Anandarao[3] and Y. D. Mayya[1]

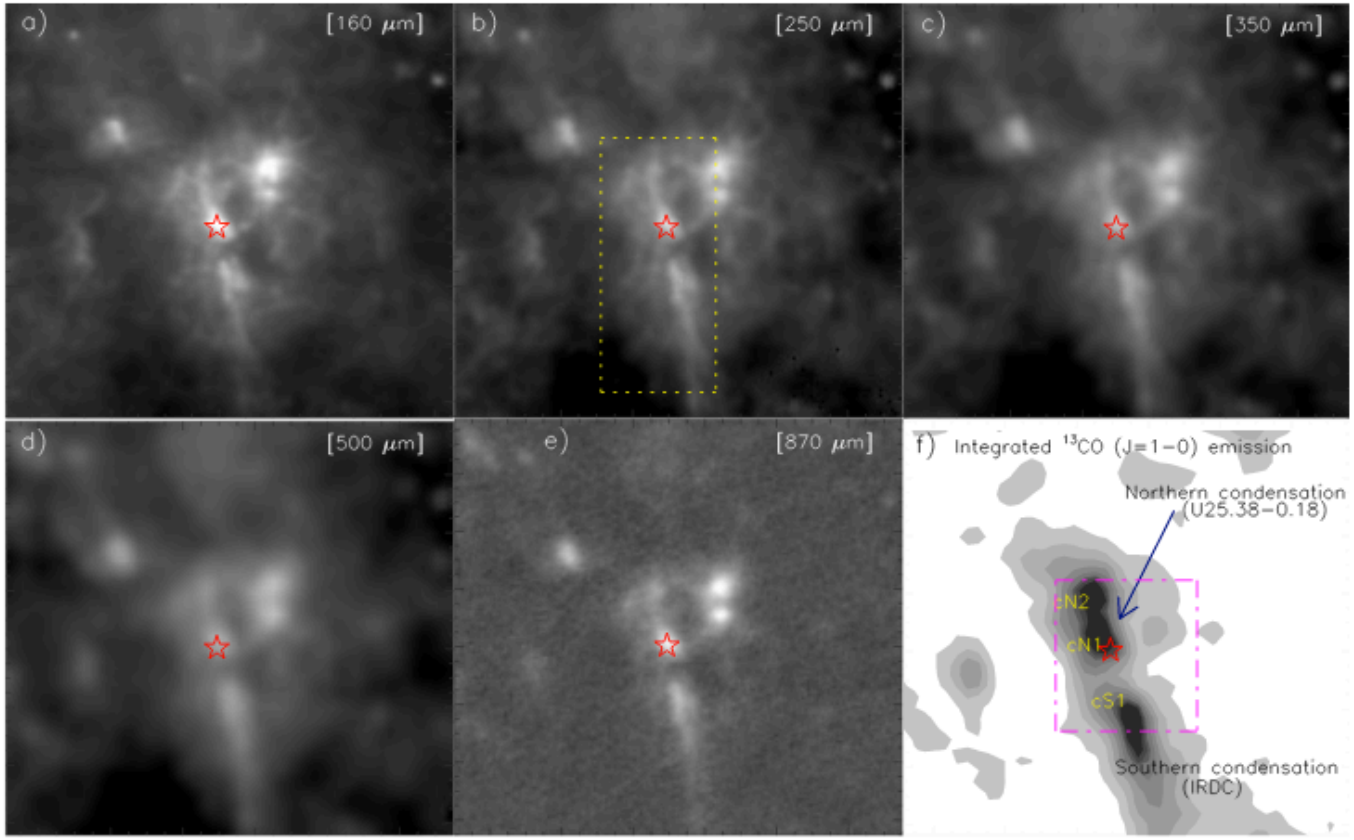

Bipolar のくびれ(filaments)
P.A. ~ 15℃

250μmでは垂直なfilamentも

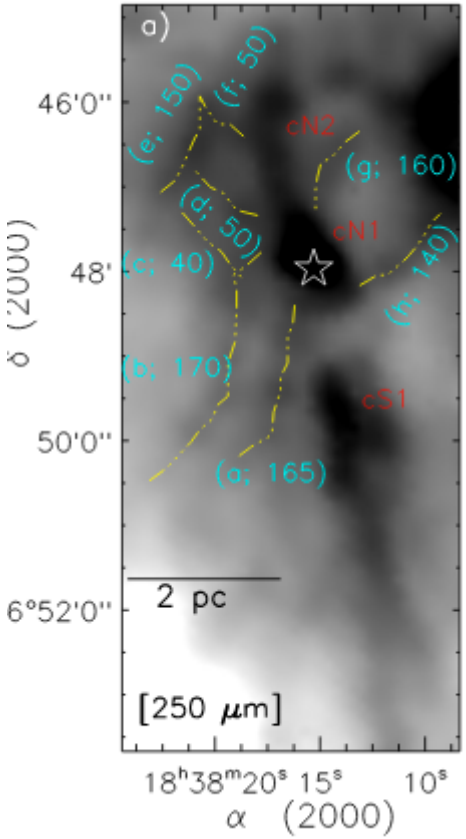

Physical environment of massive star-forming region W42

L. K. Dewangan[1], A. Luna[1], D. K. Ojha[2], B. G. Anandarao[3] and Y. D. Mayya[1]

Herschelによる温度と柱密度分布

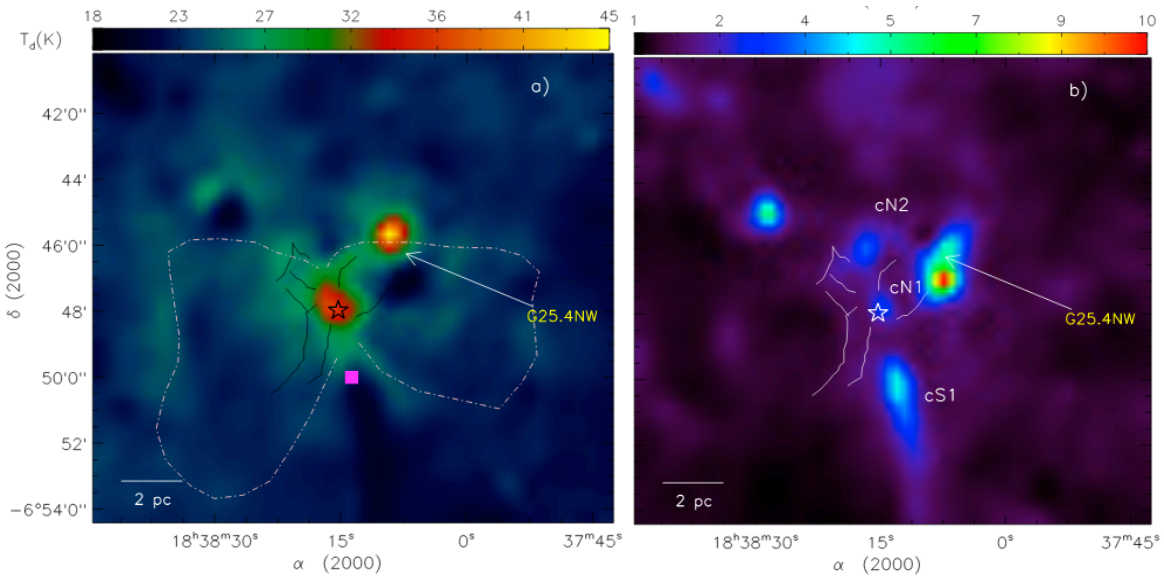

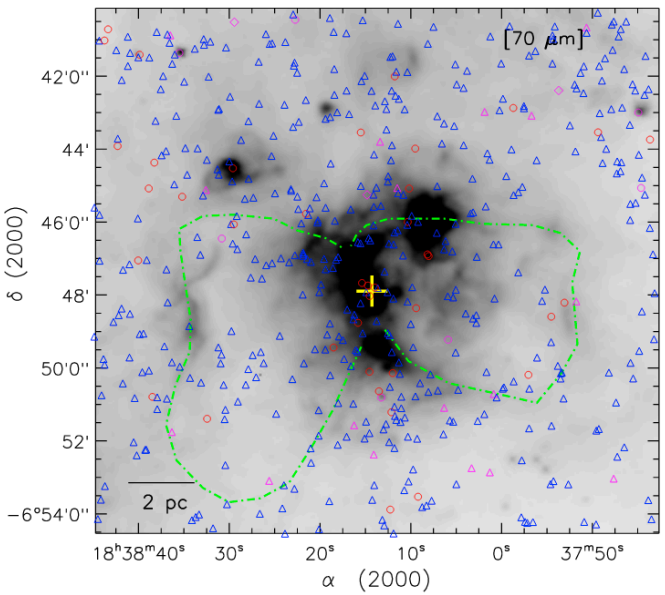

IRAC, MIPS, H-K colorでclass 0, I, II, flat, IIIを同定

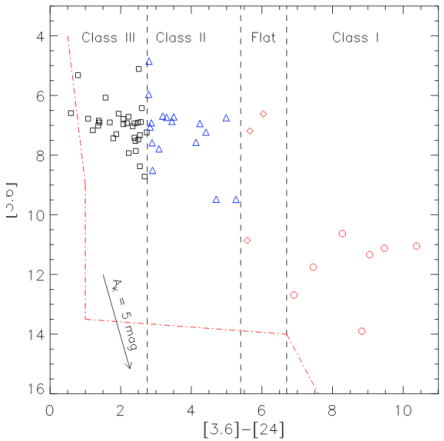

Ionized gasのcavityと13COのcavity分布が一致

Expanding velocity ~ 3 km/s

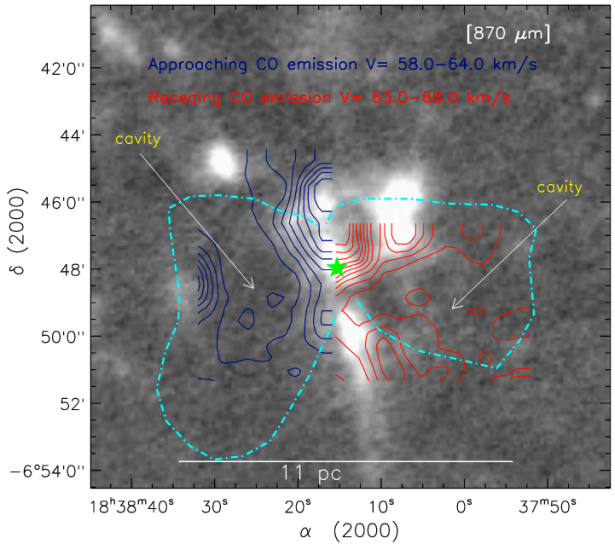

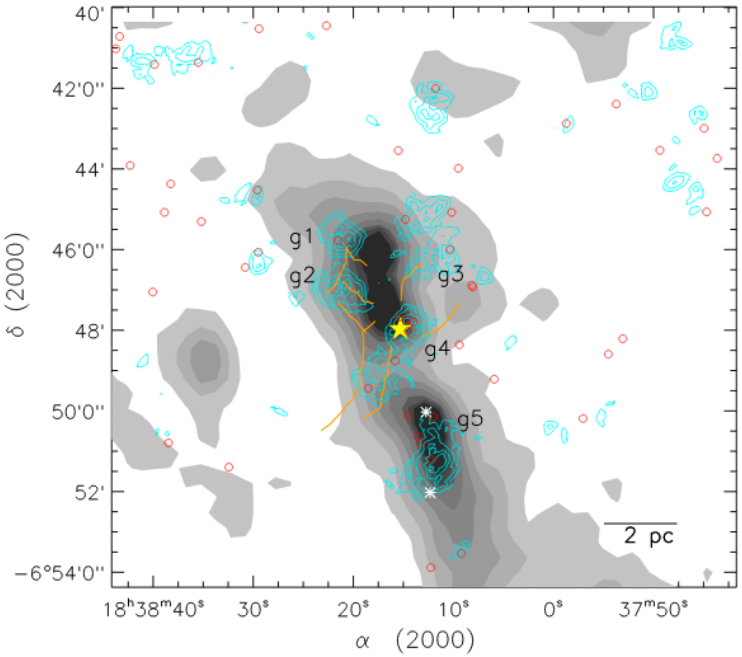

銀河磁場と同じ向き
→乱流や自己重力の影響がない

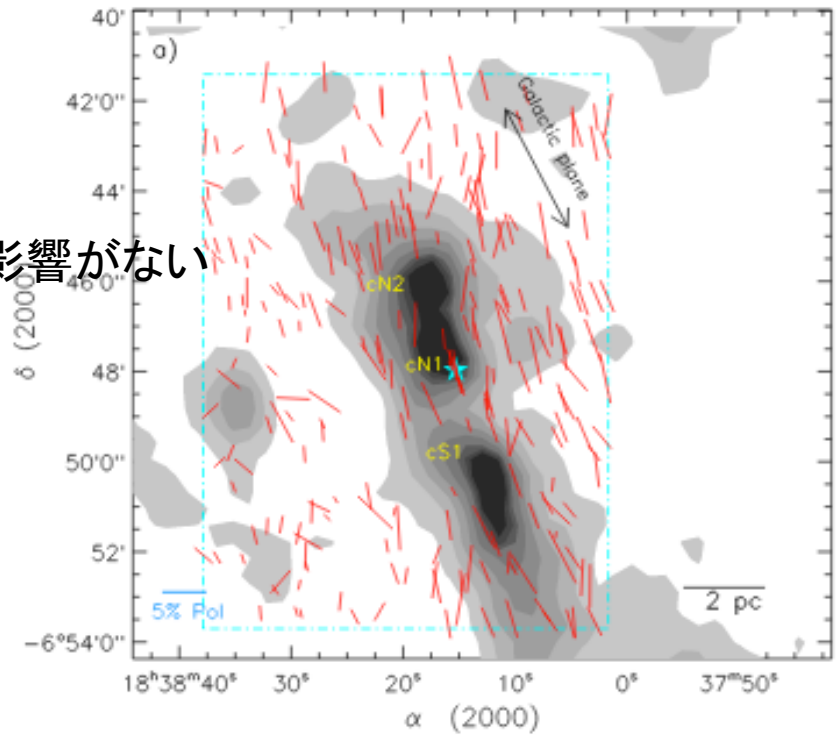

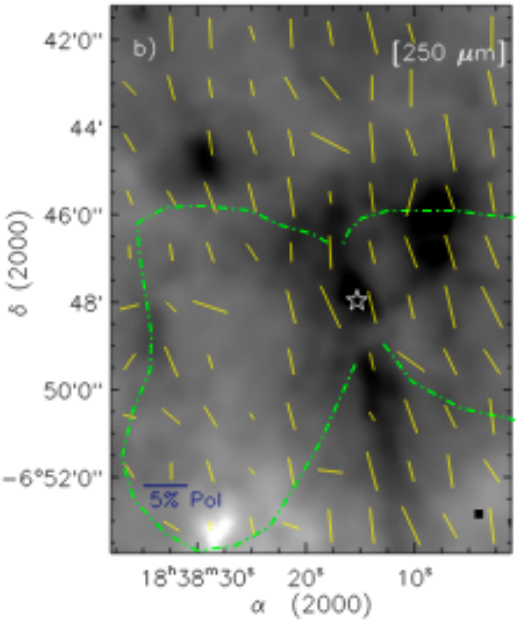

Observational Signatures of Planets in Protoplanetary Disks II: Spiral Arms Observed in Scattered Light Imaging Can be Induced by Planets

Ruobing Dong[1,2], Zhaohuan Zhu[3], Roman Rafikov[3] and James Stone[3]

Accepted by ApJ
http://arxiv.org/pdf/1507.03596

density waveを惑星を入れて形成
NIRのPIでどのように見えるか
3次元でradiative transfer を入れて計算
1Mjと6Mjが1Msunのまわりを

結果
6Mjの方がspiral armはprominent

Inner arm
Modeがm=2, 10-15°のpich angle,
180-270°まで、~150%の明るさ
→SAO 206462やMWC 758と一致

Outer arm
Tightlyに巻いていて観測と合わない
リングに見えるか、IRでようやく見える
かもしれない

等温より断熱の方が、密度ゆらぎは
小さいがPIは強い
→shockがvertical 方向へ伝わる

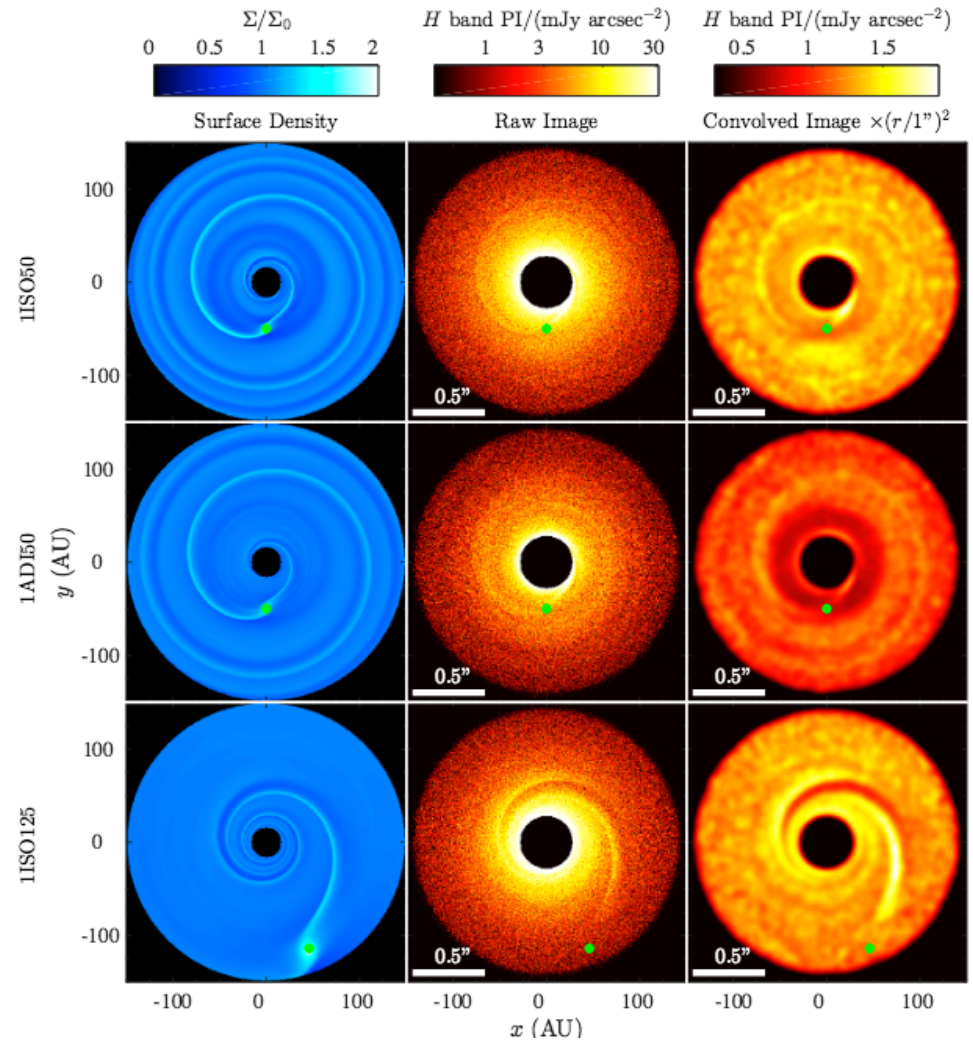

Observational Signatures of Planets in Protoplanetary Disks II: Spiral Arms Observed in Scattered Light Imaging Can be Induced by Planets

Ruobing Dong[1,2], Zhaohuan Zhu[3], Roman Rafikov[3] and James Stone[3]

計算

Atherna++ code (15 ~ 150AU)

$$T(r,z) = T_0 \left(\frac{r}{r_0}\right)^{-1/2} . \quad h = c_s/\Omega \propto r^{1.5}T^{0.5} \propto r^{1.25}$$

表面密度∝r^{-1}

Mp/Mstar

Model/Observation	EOS	q $\times 10^{-3}$	r_p AU	$(\Sigma_{wave,peak} - \Sigma_0)/\Sigma_0$ %	$(I_{wave,peak} - I_b)/I_b$ %	Radial FWHM arcsec	Pitch Angle degree
(1)	(2)	(3)	(4)	(5)	(6)	(7)	(8)
1ISO50	ISO	1	50	49(OP)	10(OP)	N/A	6(OP)
1ADI50	ADI	1	50	28(OP)	20(OP)	N/A	6(OP)
1ISO125	ISO	1	125	31(IP), 21(IS)	40(IP), 30(IS)	~ 0.09(IP), ~ 0.08(IS)	16(IP),10(IS)
6ISO50	ISO	6	50	150(OP),61(OS)	N/A	~ 0.09(OP), ~ 0.1(OS)	4(OP),2(OS)
6ADI50	ADI	6	50	77(OP), 36(OS)	190(OP)	~ 0.24(OP)	4(OP)
6ISO125	ISO	6	125	125(IP), 48(IS)	160(IP), 150(IS)	~ 0.1(IP), ~ 0.08(IS)	15(IP),10(IS)
SAO 206462[a]					~ 100 (east), ~ 300 (west)	~ 0.11(east), ~ 0.13(west)	11(east), 10(west)
MWC 758[a]					~ 200 (east), ~ 250 (west)	~ 0.07(east), ~ 0.1(west)	11(east), 10(west)

Observational Signatures of Planets in Protoplanetary Disks II: Spiral Arms Observed in Scattered Light Imaging Can be Induced by Planets

Ruobing Dong[1,2], Zhaohuan Zhu[3], Roman Rafikov[3] and James Stone[3]
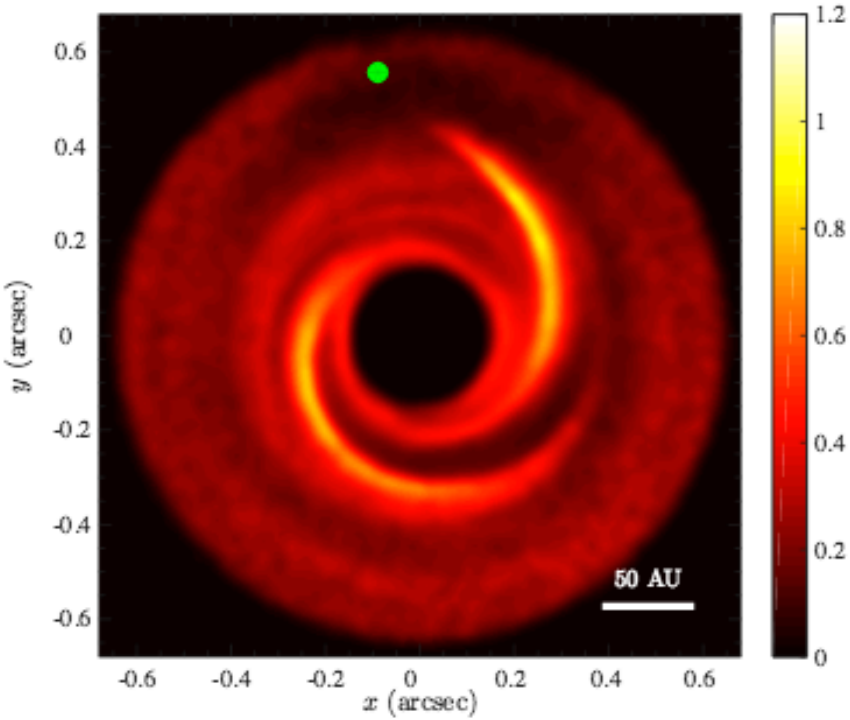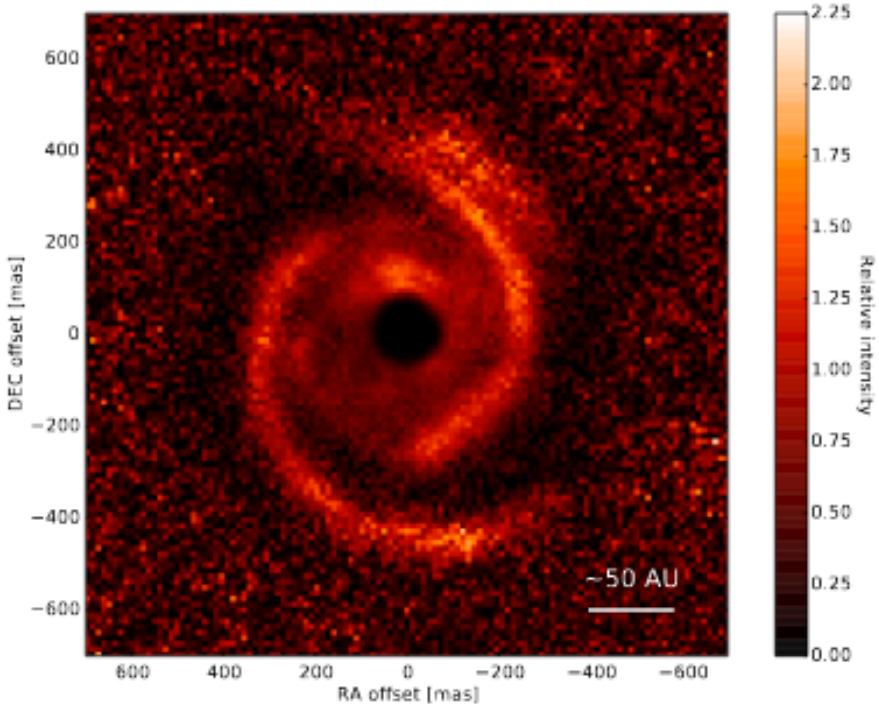
絶対値を合わせるのは難しいが、6Mjやbrown dwarfのようなmassive planetがあれば作れる。観測でdirect imaging できるかもしれない